Geochemistry, Geophysics, Geosystems

RESEARCH ARTICLE
10.1029/2021GC009654

Key Points:

- Massive deposition of carbonate nodules on a hyperarid diluvial platform in the western Qaidam Basin occurred 153–251 kyr before present
- Zoning structures in nodules were found to have distinct chemistries, crystallinities, and porosities due to fluctuant salinity of floods
- Mineralogical and isotopic analyses across the structural zones revealed substantial aqueous evolution over the nodule growth period

Supporting Information:

Supporting Information may be found in the online version of this article.

Correspondence to:

H. He,
hehp@gig.ac.cn

Citation:

Sun, Y., Li, Y., Li, K., Li, L., & He, H. (2021). Massive deposition of carbonate nodules in the hyperarid northwest Qaidam Basin of the northern Tibetan Plateau. *Geochemistry, Geophysics, Geosystems*, *22*, e2021GC009654. https://doi.org/10.1029/2021GC009654

Received 14 JAN 2021
Accepted 23 MAR 2021

Massive Deposition of Carbonate Nodules in the Hyperarid Northwest Qaidam Basin of the Northern Tibetan Plateau

Yu Sun[1,2,3], Yiliang Li[4,5], Kan Li[6], Long Li[6], and Hongping He[1,2,3]

[1]CAS Key Laboratory of Mineralogy and Metallogeny/Guangdong Provincial Key Laboratory of Mineral Physics and Materials, Guangzhou Institute of Geochemistry, Chinese Academy of Sciences, Guangzhou, China, [2]CAS Center for Excellence in Deep Earth Science, Guangzhou, China, [3]University of Chinese Academy of Sciences, Beijing, China, [4]Department of Earth Sciences, the University of Hong Kong, Pokfulam, Hong Kong, China, [5]Center for Excellence in Comparative Planetology, Chinese Academy of Sciences, Hefei, China, [6]Department of Earth & Atmospheric Sciences, University of Alberta, Edmonton, Canada

Abstract Concretionary nodule formation is a subaerial process common to both Earth and Mars. The resulting nodules contain information about particular paleoclimatic cycles. However, their genesis and the mineralogical and geochemical effects of climate change on nodule formation have not well constrained so far, limiting their applications to paleoclimatic reconstruction. Since the late Pleistocene, the Qaidam Basin in the northern Tibetan Plateau has been subjected to extreme drought, resulting in a vast area of playas with a diverse eolian morphology that resembles the surface of Mars. Recently, a massive carbonate nodule field was discovered on an ancient diluvial platform in the northwest Qaidam Basin. Detailed analyses revealed that an early period of aragonite precipitation (251 kyr before present) provided seeding material for the later growth of nodule bodies during a period of ~100 kyr. The highly unstable hydrologic and geochemical conditions during this period led to the growth of high-Mg calcite zones with varied elemental contents (e.g., Mn), crystal patterns, and porosity levels within the nodule bodies. The $\delta^{13}C$ and $\delta^{18}O$ values increased by 3‰ and 6‰, respectively, from the cores to the rims of the measured nodules. Rayleigh distillation model suggested that 50% of the H_2O and 25% of the dissolved CO_2 had been removed during nodule growth in response to the drought. These results show that nodules formed in hyperarid environments can record important hydrologic information, which may provide insights for paleo-environment studies on Mars by examining the formation of nodules in Gale Crater.

1. Introduction

Sedimentary carbonate nodules are generally millimeter-to decimeter-sized, rounded or subangular, coated carbonate assemblages that may have a concentric zoning structure (Flugel, 2004). In contrast to the soil and diagenetic carbonate concretions of various shapes that formed via the transitions of reactants in calcareous sediments and mudrocks (Mozley & Davis, 2005), carbonate nodules are found in diverse sedimentary settings on Earth, including flat seamounts, shallow subtidal settings, terrestrial flooded platforms, and palustrine wetlands (Flugel, 2004; Freytet & Verrecchia, 2002; Prager & Ginsberg, 1989; Tabor et al., 2007). Although researchers have proposed various mechanisms of carbonate nodule formation, including diagenetic concretionary cementation, bioturbation, and re-deposition, the mechanism of formation of concentrically layered structures in nodules under hyperarid climate conditions has not been identified in detail (Gregorio et al., 2018; Gregory et al., 1989; Miller et al., 2007; Rabenhorst et al., 1984).

In the terrestrial environment, diluvial platforms, and alluvial fans in arid or semi-arid climates, are favorable places for carbonate nodule formation (Alonso-Zarza & Wright, 2010; Freytet, 1973). The evaporation-induced cracking of primary sediments can provide seeding material and thus facilitate nodulization (Freytet, 1973). As liquid water evaporates and eventually disappears, the mineral deposits will evolve from carbonate to gypsum and halide (Warren, 2006). Thus, both the distribution of carbonate nodules and the change in chemical composition during nodule growth serve as important records of the late-stage evolution of water reservoirs and the deposition of sediments in arid regions (Wieder & Yaalon, 1982). However, the application of combined mineralogical and geochemical data of carbonate nodules to climatic and hydrological changes has been poorly explored so far.

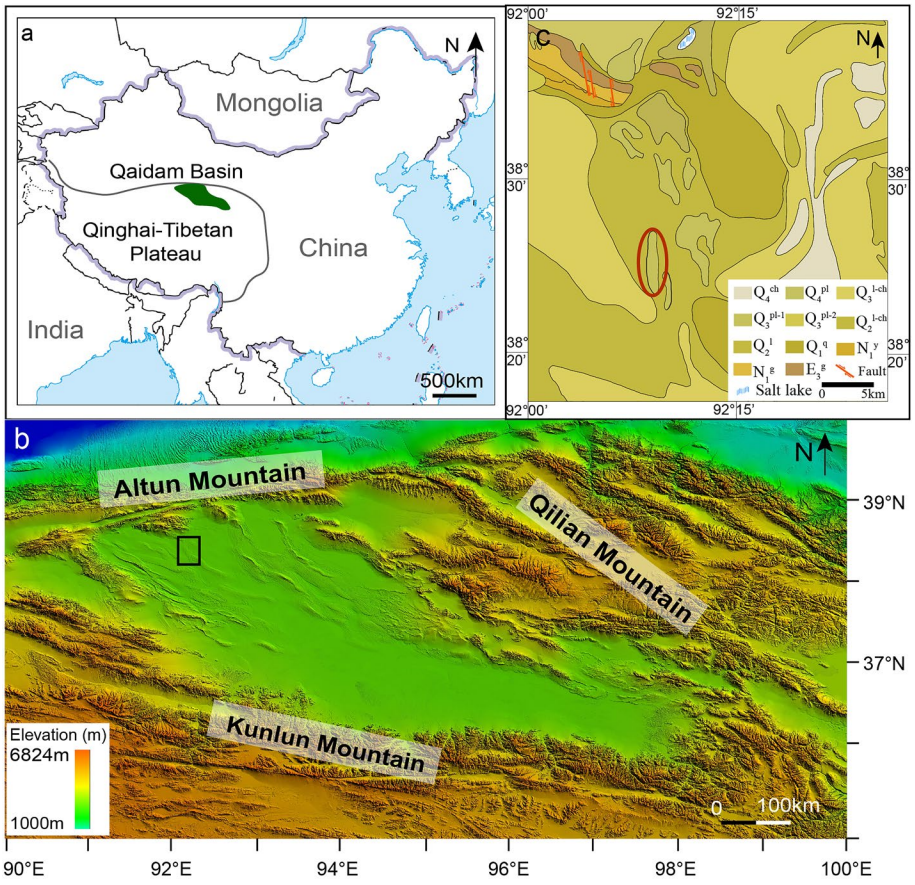

Figure 1. Geological map of the study area in the northwest Qaidam Basin (Modified from Sun et al., 2019). (a) The location (green area) of the Qaidam Basin on the Tibetan Plateau. (b) Digital elevation model map of the Qaidam Basin, with the black open square marking our study area. (c) The geological map of the study area. The red open oval marks the strata where nodule field is located. Q_4^{ch}: Chemical deposit; Q_4^{pl}: Diluvial deposit; $Q_3^{l\text{-}ch}$: Lake-chemical deposit; $Q_3^{pl\text{-}1}$: Diluvial deposit; $Q_3^{pl\text{-}2}$: Diluvial deposit; $Q_2^{l\text{-}ch}$: Lake-chemical deposit; Q_2^{l}: Lake deposit; Q_1^{q}: Qigequan Formation (Fm.); N_1^{y}: Xiayoushashan Fm.; N_1^{g}: Shangganchaigou Fm.; E_3^{g}: Xiaganchaigou Fm.

The Qaidam Basin (area: ~700 × 300 km^2; Figure 1a), which is located in the northern Tibetan Plateau, has been subject to extreme drought for the past 0.6 Ma due to the rise of the Tibetan Plateau (Han et al., 2014). Surrounded by mountains with altitudes >5,000 m, the basin floor is approximately 2,800–3,300 m above sea level (Kong et al., 2018). The basin has had a consistently high evaporation to precipitation ratio, with current levels of 2,590 and <20 mm, respectively, in the western basin area (Kong et al., 2018). Playa deposits as thick as 2,000–3,500 m have accumulated in the basin (Han et al., 2014), and perennial wind erosion over a vast area of these deposits has produced diverse eolian landscapes associated with evaporites. Consequently, the Qaidam Basin is considered one of the largest Mars analogs on Earth (Anglés & Li, 2017; Kong et al., 2018; Sun et al., 2019; Xiao et al., 2016).

Here, we report our discovery of a massive deposition of carbonate nodules in the northwest Qaidam Basin. We carried out detailed investigations of the mineralogy, petrology, and elemental and isotopic compositions of these carbonate nodules with the aim of understanding the formation of the nodular structures and exploring whether these structures could elucidate the water cycle in a diluvial environment within a hyperarid climate. Furthermore, nodules have been discovered in several places on Mars, especially in the Gale Crater (Stack et al., 2014; Wiens et al., 2017). As very little geochemical data can be obtained from the Gale nodules at present, the environmental evolution during the period of nodule growth has not been fully explored, particularly with regard to the water cycle and its impact on habitability. This study of nodules from an analogous environment on Earth may provide insights into the origins of possible primary carbonate nodules (Yoshida et al., 2018) and a better understanding of the paleo-environment on Mars.

2. Samples and Methods

2.1. Geological Background

In the northwest Qaidam Basin (Figure 1), nodules are found in the upper Pleistocene strata, which are composed of lacustrine sediments and diluvial deposits that were formed during the late stage of evolution of salt lakes (Han et al., 2014). Our samples were collected from a diluvial platform in the basin (marked by a red circle in Figure 1c) located in the piedmont of the Altun Mountain.

At 38°27′N, 92°9′E, 30 nodule samples were collected from both surface exposures and from road cuts and dug ditches down to 1 m below the surface. 10 nodules with diameters ranging from 5 to 15 cm were selected for detailed analyses.

2.2. Methods

The mineralogy of the nodules was characterized using a D8 Advance X-ray diffractometer (Bruker), a JXA-8230 electron probe microanalyzer (JEOL), an SU8010 cold field emission scanning electron microscope (FESEM, Hitachi, Japan) equipped with an energy dispersive X-ray spectrometer (AMETEK-EDAX, USA), and an FEI Talos F200S transmission electron microscope at the Guangzhou Institute of Geochemistry, Chinese Academy of Sciences (Guangzhou, China).

The nodules were cut in half to expose the internal zoning structures. Samples from different zones were collected by micro-drilling and ground into powder for X-ray diffraction (XRD) analysis. The XRD patterns were measured between 5° and 60° (2θ) at a scanning rate of 2° (2θ) min^{-1} on the Bruker X-ray diffractometer with Ni-filtered CuKα radiation (λ = 0.154 nm; 40 kV and 40 mA). Thin sections of the nodules that retained the complete zoning structures were made for electron probe microanalysis (EPMA) measurements and backscattered electron (BSE) imaging. Secondary electron image observation of pieces from different layers was performed using scanning electron microscopy. X-ray fluorescence spectroscopy mapping (μ-XRF) of cross-sections of the nodules was performed using a Bruker M4 TORNADO device equipped with an Rh X-ray source at Northwest University (Xi'an, China). For the analysis, the X-ray tube settings were 50 kV and 199 μA, the samples were measured at a pressure of 20 mbar, and the step size and integration time per pixel were set to 55 μm and 5 ms, respectively.

The carbon and oxygen isotopic compositions of the nodules were measured at the University of Alberta (Edmonton, AB, Canada). Powdered samples from multiple zones of individual nodules were reacted with 100% orthophosphoric acid in glass tubes overnight at 25°C under a vacuum to liberate CO_2 gas, which was then cryogenically purified and collected into sample tubes and measured using the dual-inlet mode in a Thermo Finnigan MAT 253 isotope ratio mass spectrometer. An acid fractionation correction was applied to aragonite. The analytical error was 0.2‰ (2σ) for both $\delta^{13}C$ and $\delta^{18}O$, which are reported relative to the Vienna-PDB standard.

The U and Th concentrations and isotopic compositions were measured using a Thermo Neptune multicollector–inductively coupled plasma–mass spectrometer at Xi'an Jiaotong University (Xi'an, China; Text S1). The ^{230}Th ages were calculated following the method of Cheng et al. (2013).

3. Results

3.1. Distribution of Nodules

In the basin, the nodules are distributed in a narrow strip measuring approximately 10 km long and 2.5 km wide (Figures 1c and 2a). The nodule field is flat, and its surface is covered with small dunes and eolian debris (Figures 2a and 2b). The intact nodules are mostly buried by wind-introduced sands (during a later period) and weathered nodule fragments (Figure 2e), which aggregate as dunes (Figure 2b). The exposed nodules are either loose or cemented by gypsum in the shapes of dunes (Figure 2b) and small stakes (Figure 2c). The nodules vary in diameter from 1 cm to more than 12 cm (Figures 2b–2d). The unique inner structures, which appear as concentric layers around a core, are exposed in some weathered nodule fragments (Figures 2c and 2d). In some cases, groups of several small nodules later grew into single large nodules (Figure 2f).

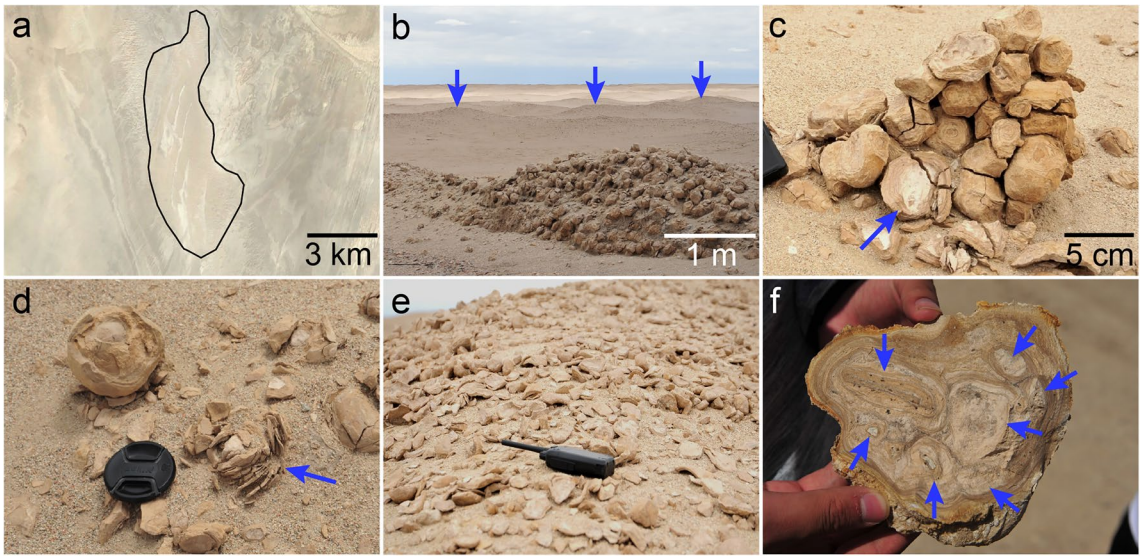

Figure 2. The nodule field and petrological structures of nodules. (a) The distribution area of nodules, circled by black line (Longitude from 92°07′57″ to 92°10′19″, Latitude from 38°30′52″ to 38°25′26″). (b) Cross-section of a dune showing cemented nodules inside. Every dune (blue arrows) is composed of nodules cemented by gypsum and halite between nodule aggregates. (c) A small cemented nodule stake with partially weathered nodules exposing the zoning structure (blue arrow). (d) Broken and partially weathered nodules with separated layers filled by smaller weathered debris. (e) Numerous nodules were weathered into fragments on the surface. (f) A big nodule grew from multiple small nodules, with a core at various size in each one (blue arrows).

3.2. Mineralogy and Petrology of Nodules

A detailed examination of the cross-section of a nodule revealed seven layers with distinct colors (Figure 3a). The mineral compositions of these layers, however, yielded the same bulk XRD measurement patterns (Figure 3b), which are consistent with that of calcite but display an obvious peak shift. The replacement of Ca by Mg in the crystal structure would shift the $d_{(104)}$ peak from calcite toward dolomite. In the patterns yielded by our samples, the main peak lies between the calcite and dolomite peaks (Figure 3b), indicating that the nodule layers are composed of high-Mg calcite. Utilizing a previously published relationship between 2-theta shift and calcite Mg/Ca ratio (J. Ries, 2011), the Mg/Ca ratio of the high-Mg calcite is calculated to be 0.33. The XRD patterns of minerals in the nodule core show that aragonite is the predominant mineral with minor detrital quartz and feldspar, and evaporites (e.g., halite and gypsum) (Figure 3c). Halite and gypsum also appear in every layer with varying abundances.

Eight nodules were analyzed by EPMA to further verify the chemical compositions of the carbonate minerals. Every nodule was again divided into different layers based on color. The results (Table S1) show that the Mg/Ca atomic ratios ranged from 0.1 to 0.6, with an average value of 0.34, similar to the XRD result. The average Mg/Ca ratios of the individual nodules varied from 0.27 to 0.44. However, no obvious trend in the Mg/Ca ratio was observed across the zoning structure.

Although the different layers were found to have almost identical mineral compositions, they varied in color from brown in thinner layers to light yellow in relatively thick layers (Figure 4a). The brown thin layers were more compact and the light yellow layers were more porous, as demonstrated by the epoxy resin-filled dark areas in the BSE images (Figure 4b). The micro-morphology of the carbonate mineral in the light-yellow layers uniquely shows that rhombs stack up along *c*-axis to form pinecone-shaped aggregates (Figure 4c). The rhombic aggregates were mostly 1–2 μm in size and composed of nanoparticles (Figure 4e). Some of the rhombic aggregates grew directly on the surfaces of other detrital minerals, such as quartz (Figure 4d). Carbonates from the brown layers, however, displayed poor crystallinity (Figure 4f).

μ-XRF mapping was used to examine the elemental distributions in different layers of the nodules. No obvious Ca and Mg zoning structure was observed in the samples (Figures 4g and 4h), whereas a striking Mn zoning structure was apparent (although at very low contents of 0.41 atom % on average), with more Mn enrichment in the thick light yellow layers than the thin brown layers (Figure 4i). To a lesser extent, Fe, Si,

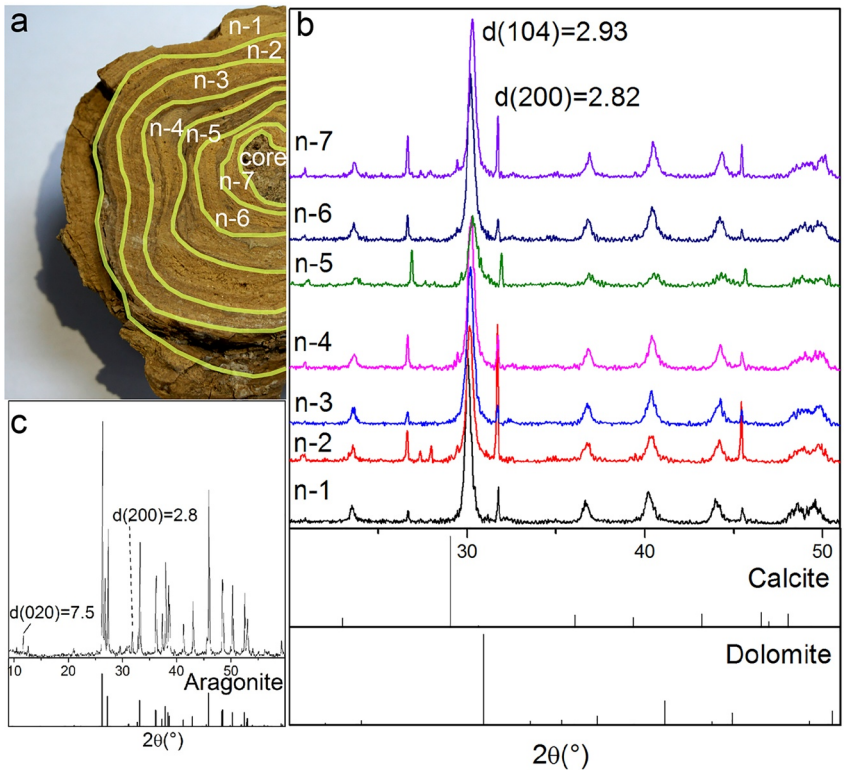

Figure 3. X-ray diffraction analyses of a nodule sample. (a) The cross-section of the studied nodule, which was divided into seven layers based on the color change. (b) XRD patterns of the seven layers. The dominated mineral is calcite. Halite is identified by the $d_{(200)}$ peak. Different layers display the same mineral compositions. (c) The core is identified as aragonite with minor gypsum and halite. Halite and gypsum are identified by their $d_{(200)}$ and $d_{(020)}$ values.

and Al also exhibited parallel zoning structures, suggesting the occurrence of silicate in the core and some layers (Figure S1).

3.3. Stable Isotopic Compositions and ^{230}Th-Dating Ages

The internal layers of four nodules were separated for $\delta^{13}C$ and $\delta^{18}O$ analyses (Table S2). The strong ^{18}O enrichment in the nodule carbonates (Figure 5) indicated formation from highly evaporated water (Han et al., 2014). Although isotopic variations were observed among different nodules, the isotopic compositions of both $\delta^{13}C$ (up to 3‰) and $\delta^{18}O$ (up to 6‰) in each nodule exhibited consistently increasing trends from the core to the rim (Figure 5).

We modeled these data assuming that an isotope fractionation equilibrium was reached during the precipitation of carbonate from water (Emrich, 1970) and that the degassing of H_2O and CO_2 from the water also occurred with kinetic isotope fractionation (Kakiuchi & Matsuo, 1979; Kim & O'Neil, 1997; Mook et al., 1974; Text S2). The average summer temperature of ~15°C in the western Qaidam Basin (Kong et al., 2018) was used in the model.

The modeling results are shown in Figure 5. The $\delta^{13}C$ and $\delta^{18}O$ values of carbonate in the nodule lie between the two dashed red lines modeled from the lowest and highest $\delta^{18}O$ values. From the figure, we can infer that during nodule growth from the core to the rim, up to 50% of H_2O and 25% of CO_2 could have been removed from the water reservoir by evaporation.

^{230}Th dating was applied to both the core carbonate (-c) and outmost layers (-o) of three nodules (Table S3). The ages of the cores were 231 ± 8 kyr before present (BP), 244 ± 24 kyr BP, and 251 ± 9 kyr BP, and the ages of the outmost layers were 153 ± 4 kyr BP, 191 ± 10 kyr BP, and 198 ± 6 kyr BP. The growth durations of individual nodules ranged from 33 to 91 kyr.

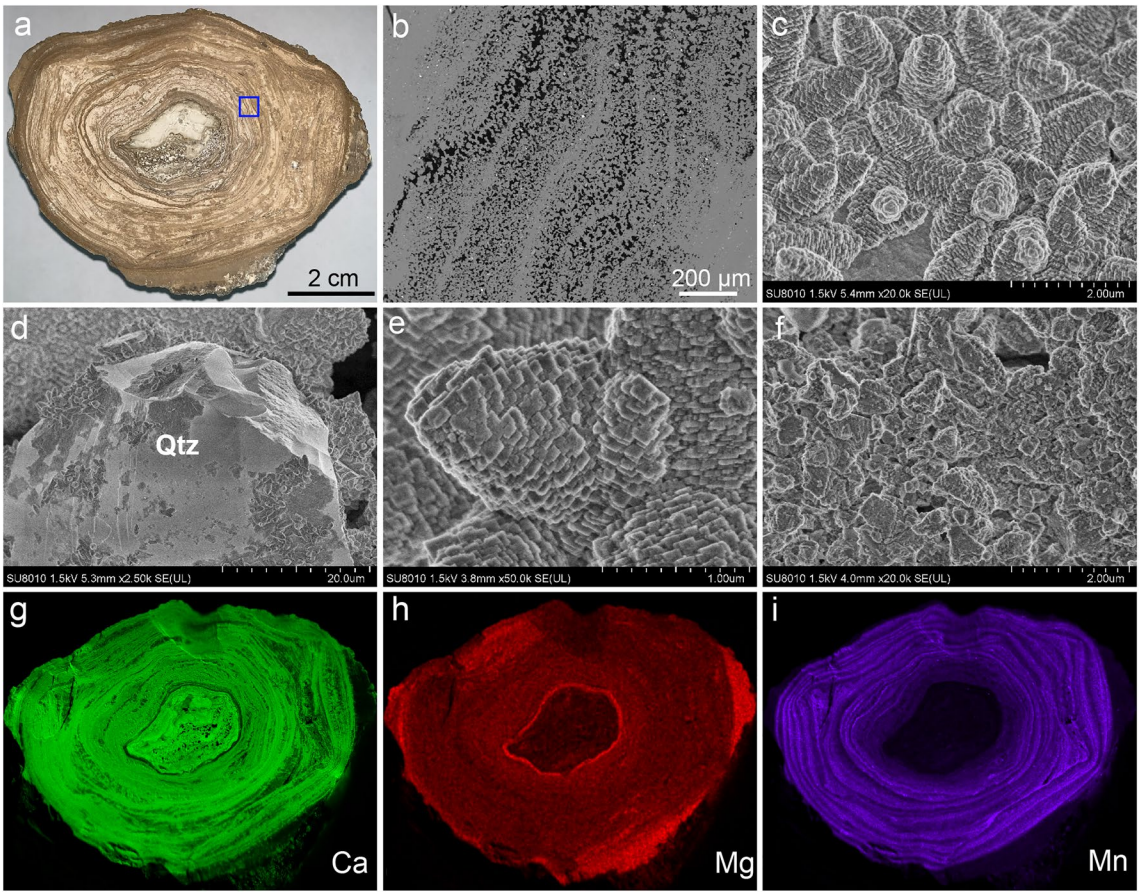

Figure 4. Petrography, mineral crystal morphology, and element distribution of the zoning structure of nodules. (a) The cross-section of the nodule. (b). BSE image of the zoning structure in an area marked by the blue open square in Figure 4(a), showing the light yellow layers are more porous and the brown layers are more compact. (c) Pinecone-shaped aggregates of carbonate from the light yellow layers. (d) Pinecone-shaped aggregates of carbonate on detrital quartz. (e) Stacking of carbonate nanoparticles forms the aggregates. Nanoparticles assemble into rhombus pieces, which further form the pinecone-shaped aggregates. (f) Carbonate aggregates from the brown layers. (g) The distribution of Ca in the nodule. (h) The distribution of Mg in the nodule. (i) The distribution of Mn in the nodule.

4. Discussion

4.1. Paleoclimate Reconstruction by the Mineralogy and Isotopic Compositions of Carbonate Nodules

Diluvial platforms are usually flat with poor drainage and may flood seasonally to perennially (Rieser et al., 2005), producing a favorable environment for carbonate nodule formation (Driese & Mora, 1993; Freytet, 1973; Tabor et al., 2007). The nodules in the western Qaidam Basin were formed on an ancient diluvial platform in front of Altun Mountain. The cores of these nodules are composed mainly of aragonite, with minor amounts of detrital quartz, feldspar, and clay minerals (chlorite, kaolinite, and illite; Figure S2). Because aragonite is metastable in epigenic environments (Boettcher & Wyllie, 1968), the preservation of this mineral indicates that these nodules have been well preserved in the water-deficient environment and thus retained their pristine signatures since the formation of the core material (Németh et al., 2018). The layers surrounding the nodule cores are composed of high-Mg calcite. The Mg/Ca ratio and temperature are the two main factors controlling aragonite and calcite precipitation (Morse et al., 2007; J. B. Ries, 2004). As a significant change in temperature over a relatively short time interval from 250 to 150 kyr is unlikely, the observed mineralogical changes in the nodules should be attributed to an Mg/Ca shift between the formation of the core material and the growth of the nodules. The study of the aqueous chemistry of the nearest modern salt lake in the Dalangtan area (distance from the study site: 60 km) indicates that the water is enriched in Mg (maximum Mg/Ca ratio = 3.1; Kong et al., 2018). At such a high Mg/Ca ratio, an average temperature

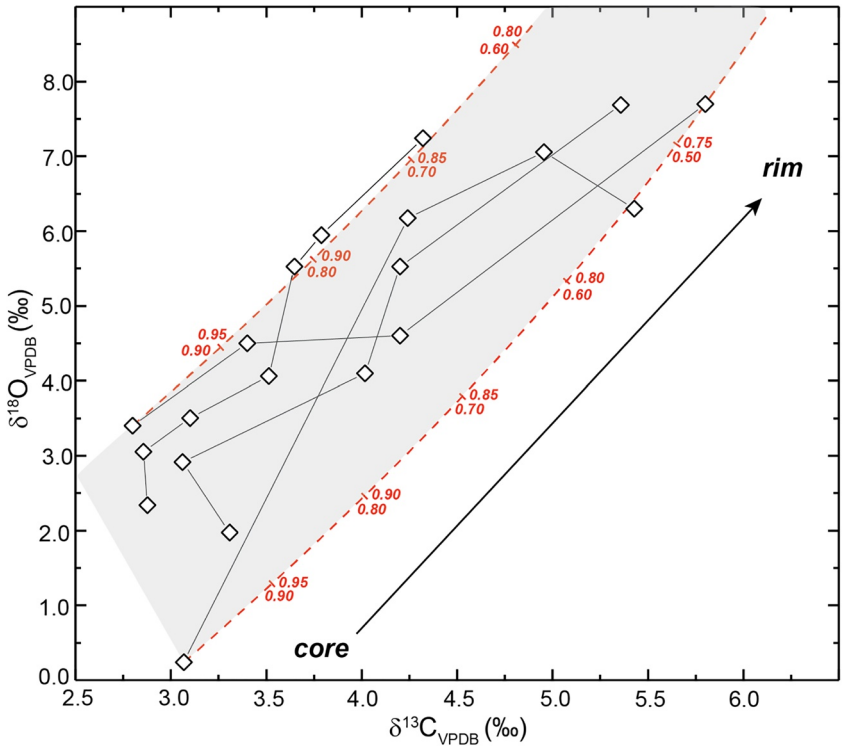

Figure 5. Rayleigh distillation model of the $\delta^{13}C$ and $\delta^{18}O$ values from the core to the rim of four carbonate nodule samples as a result of H_2O and CO_2 degassing at 15°C. Each group of linked empty diamonds represents the data from core to rim data of one nodule. The two red dashed lines are the best-fitted lines to encompass the measured data. Numbers along these two lines are the remaining fractions (f) of CO_2 (the upper number) and H_2O (the lower number) in the reservoir.

of 15°C would be favorable for aragonite formation (Morse et al., 2007). A lower Mg/Ca ratio is needed to shift the mineral precipitation from aragonite to calcite (Morse et al., 2007). Because progressive aragonite precipitation would result in a higher Mg/Ca ratio, a reduction in the Mg/Ca ratio could only be achieved by an increased influx of water (and thus a less dry climate) with a low Mg/Ca ratio (J. Ries, 2011). In the studied region, the source of this influx may have been surface water from the surrounding mountains (Yang et al., 2016). This speculated period of relatively low aridity is consistent with the regional geological record in the basin (Han et al., 2014; Yang et al., 2016). Previously, a detailed examination of the sedimentary facies of a 938.5-m-long drill core (SG-1) in our study area revealed that the perennial saline lakes were replaced by ephemeral playa salt lakes since 0.6 Ma, indicating that floods of varying severity could have flowed from the nearby mountain during this period (Han et al., 2014).

The $\delta^{13}C$ and $\delta^{18}O$ values in each nodule exhibited strong covariation from the core to the rim, indicating that a single environmental factor could have controlled the stable carbon and oxygen isotopic compositions along with the nodule growth (Candy et al., 2012; Han et al., 2014). Previous studies of the SG-1 drill core demonstrated an obvious correlation between the increasing $\delta^{13}C$ and $\delta^{18}O$ values of post-0.6 Ma carbonates (Han et al., 2014). The temperature did not change significantly during this period and thus could not have played a substantial role in the fractionation of the stable carbon and oxygen isotopic compositions. Consequently, changes in the water budget in response to aridity should be the main environmental driver of the observed isotopic shifts (Han et al., 2014). Consistently, the carbon and oxygen isotopic co-variations in the carbonate nodule evidently indicate sustained aridity in the northwestern Qaidam Basin during the formation stage from 251 to 153 kyr BP, although this was a less dry period relative to the other period.

Accordingly, we can infer that in the late Pleistocene, the primary lake water in the piedmont of the Altun Mountain created a high-Mg aqueous environment from which aragonite was precipitated. As the climate shifted toward slightly wetter conditions, the increased water input decreased the Mg/Ca ratio in the

aqueous environment and induced the deposition of high-Mg calcite. Overall, the sustained drought across the basin induced prolonged water evaporation and carbonate deposition; the latter could have produced H^+ to slightly decrease the pH of water and consequently induce CO_2 degassing. These two quantifiable processes can be described by:

$$Ca^{2+} + 2HCO_3^- \rightarrow CaCO_3 + CO_2 \uparrow + H_2O$$

These processes together led to the correlated increases in $\delta^{18}O$ of the lake water and $\delta^{13}C$ of dissolved inorganic carbon (Talbot, 1990), which were transferred to carbonate in the nodule. Rayleigh distillation modeling of the nodule isotopic data (Figure 5) suggests the degassing of up to 50% of water and 25% of dissolved inorganic carbon during nodule growth. This aqueous environment and paleoclimate suitable for carbonate nodule formation persisted for ~100 kyr. During this period, the water evaporation sometimes could be significant enough to induce gypsum precipitation. This indicates that significant HCO_3^- removal due to carbonate deposition and/or CO_2 degassing has resulted in a condition of $mHCO_3^- << mCa^{2+}$ (Hardie, 2003). The continuous increase in water salinity eventually led to a shift in the mineral precipitation from carbonate to evaporative salts, which cemented the nodules (Eugster, 1980).

4.2. The Formation of Zoning Structure in Nodule

The Qaidam nodules are characterized mainly by a prominent zoning structure surrounding a core. The core material may have formed from evaporation-induced cracked fragments of primary carbonate that precipitated around 230–250 kyr BP and provided seeding material for later carbonate precipitation (Alonso-Zarza & Wright, 2010; Freytet, 1973). High seasonal levels of water influx in later years facilitated the precipitation of high-Mg calcite around previous sediment fragments to form the nodular structure (Freytet, 1973).

Transmission electron microscopy–energy dispersive X-ray spectroscopy mapping revealed that on a nano-scale, Mn is distributed with Ca and Mg in the carbonate (Figure S3); in other words, Mn is present mostly in the lattice of high-Mg calcite (Driese & Mora, 1993; Sancheznavas et al., 2009; Figure S3). The fluctuations in the Mn content clearly show that the water reservoir was unstable and strongly affected by water influx. At higher degrees of supersaturation, more Mn would be incorporated into the calcite crystal structure, and the calcite crystallization rates would increase (Sancheznavas et al., 2009). This would result in the stacking of steep rhombs along the *c*-axis, a common feature of calcite formed in hypersaline environments (Given & Wilkinson, 1985). The light yellow layers are more porous due to larger aggregates of carbonate crystals and rapid rates of growth, with a higher Mn content, better crystallinity, and higher porosity. These thick layers indicate higher water salinity, whereas the brown layers indicate lower salinity. In an oxidizing environment, carbonate typically displays an earthy yellow color (Flugel, 2004), whereas a more compact structure can darken the material to a nearly brown color. Therefore, the color change is controlled by the aqueous condition and is thus another index of climate change—variations in the zoning structure between the light yellow layers and the brown layers reflect second-order climatic oscillations with hundred-to thousand-year cycles in a long-term, first-order persistent dry climate over hundreds of thousands of years.

4.3. Implication for Nodules on Mars

The morphological, mineralogical, and geochemical data suggest that increased seasonal/perennial water influxes were responsible for nodule formation in the northwest Qaidam Basin. During the formation of the carbonate nodules in the diluvial platform, the ancient salt lake continued to shrink and eventually disappeared from the piedmont, after which only flood-driven wet–dry cycles occurred in the nodule deposition area over 150–250 kyr (Han et al., 2014). Persistent drought made the surface conditions increasingly uninhabitable and eventually left the surface exposed to heavy eolian carving after nodule formation. Particularly, numerous nodules have been fragmented by strong weathering and are exposed to the surface with other detrital particles (Figure 2e).

The Curiosity rover has discovered several occurrences of millimeter to centimeter nodules and concretions in the Gale Crater on Mars (Stack et al., 2014; Wiens et al., 2017). Most of these nodules and concretions

are highly weathered, and some even left with only spherical voids (Stack et al., 2014; Wiens et al., 2017). The locations of the Gale nodules are mostly related to alluvial or fluvial fans (Wiens et al., 2017). The Gale nodules are proposed to have formed from permeable sediments, active water systems, and supersaturated fluids (Stack et al., 2014). This would suggest similar formation scenarios of the Gale and Qaidam nodules, despite differences in size that could be attributed to differences in diffusion coefficients, solute concentrations, and CO_2 solubility (Yoshida et al., 2018). Although some of the Martian nodules are iron-rich, Yoshida et al. (2018) suggested that their genesis was a process in which primary carbonate nodules were altered by iron-rich acidic fluids. The possible occurrence of carbonate nodules on the Martian surface implies that a diverse aqueous environment could have resulted in an agitated hydrologic system during the late stage of the water evolution on the Martian surface.

Under current conditions, surface liquid water is rarely observed in either the northwest Qaidam Basin or Mars. However, the well-developed ancient diluvial deposits on both surfaces indicate the existence of ancient surface water influx (Yang et al., 2016), which might mediate the growth of those nodules. Although the detailed inner structures and geochemical features of the Gale nodules are unknown, this study of the Qaidam nodules implies that on ancient Mars, some periods might have been characterized by surface conditions that favored the formation of potential carbonate nodules. Such conditions could have also sustained a late-stage habitable environment.

5. Conclusions

A 10 × 2.5-km^2 field of carbonate nodules was discovered on a diluvial platform in the northwestern Qaidam Basin. In this study, the nodules were shown to exhibit strongly variable morphological, mineralogical and geochemical features from the core to the rim, indicating fluctuating hydrological conditions during nodule growth in response to short-term (second-order) climatic changes in a long-term (first-order) persistent hyper-arid climate over a period from 251 to 153 kyr BP. The results of modeling the stable carbon and oxygen isotopic compositions suggest that up to 50% H_2O and 25% of dissolved inorganic carbon could have been removed due to the persistent drought. These results demonstrate that carbonate nodules can record important hydrologic information in hyperarid–semiarid environments. Given the analogous geological settings and key factors controlling the formation of the Qaidam nodules and the nodules identified on Mars, it is possible that the Martian nodules might be a record of key information about the late-stage evolution of aqueous environments on the Martian surface.

Data Availability Statement

Research Data associated with this article can be accessed at https://data.mendeley.com/datasets/n8cjmmd5jf/1.

Acknowledgments
We thank Professor Jinhua Li from Institute of Geology and Geophysics, Chinese Academy of Sciences for his very kind help in μ-XRF mapping of the whole nodule specimens. This work was supported by the National Key R&D Program of China (Grant No. 2017YFC0602306), the National Natural Science Foundation of China (Nos. 42072044, 41530313, and 41825003), Key Research Program of Frontier Sciences, CAS (Grant No. QYZDJ-SSW-DQC023), and the Strategic Priority Research Program of Chinese Academy of Sciences (No. XDB41000000).

References

Alonso-Zarza, A. M., and Wright, V. (2010). Palustrine carbonates. In A. M. Alonso-Zarza, L. H. Tanner (Eds.), Developments in Sedimentology (Vol. 61, pp. 103–131). Elsevier.

Anglés, A., and Li, Y. (2017). The western Qaidam Basin as a potential Martian environmental analogue: An overview. *Journal of Geophysical Reserach Planets*, *122*, 856–888. https://doi.org/10.1002/2017je005293

Boettcher, A. L., & Wyllie, P. J. (1968). The calcite-aragonite transition measured in the system CaO-CO_2-H_2O. *The Journal of Geology*, *76*(3), 314–330. https://doi.org/10.1086/627331

Candy, I., Adamson, K., Gallant, C. E., Whitfield, E., & Pope, R. (2012). Oxygen and carbon isotopic composition of quaternary meteoric carbonates from western and southern Europe: Their role in palaoenvironmental reconstruction. *Palaeogeography, Palaeoclimatology, Palaeoecology*, *326–328*, 1–11. https://doi.org/10.1016/j.palaeo.2011.12.017

Cheng, H., Lawrence Edwards, R., Shen, C.-C., Polyak, V. J., Asmerom, Y., Woodhead, J., et al. (2013). Improvements in 230Th dating, 230Th and 234U half-life values, and U-Th isotopic measurements by multi-collector inductively coupled plasma mass spectrometry. *Earth and Planetary Science Letters*, *371–372*, 82–91. https://doi.org/10.1016/j.epsl.2013.04.006

Driese, S. G., & Mora, C. I. (1993). Physico-chemical environment of pedogenic carbonate formation in Devonian vertic palaeosols, central Appalachians, USA. *Sedimentology*, *40*(2), 199–216. https://doi.org/10.1111/j.1365-3091.1993.tb01761.x

Emrich, K., Ehhalt, D. H., Vogel, J. C. 1970). Carbon isotope fractionation during the precipitation of calcium carbonate. *Earth and Planetary Science Letters*, *8*(5), 363–371. https://doi.org/10.1016/0012-821x(70)90109-3

Eugster, H. P. (1980). Geochemistry of Evaporitic Lacustrine Deposits. *Annual Review of Earth and Planetary Sciences*, *8*(1), 35–63. https://doi.org/10.1146/annurev.ea.08.050180.000343

Flugel, E. (2004). *Microfacies of Carbonate Rocks*. Springer.

Freytet, P. (1973). Petrography and paleo-environment of continental carbonate deposits with particular reference to the upper cretaceous and lower eocene of languedoc (Southern France). *Sedimentary Geology*, *10*(1), 25–60. https://doi.org/10.1016/0037-0738(73)90009-2

Freytet, P., & Verrecchia, E. P. (2002). Lacustrine and palustrine carbonate petrography: an overview. *Journal of Paleolimnology*, *27*(2), 221–237. https://doi.org/10.1023/a:1014263722766

Given, R. K., and B. H. Wilkinson, (1985). Kinetic control of morphology, composition, and mineralogy of abiotic sedimentary carbonates. *Journal of Sedimentary Research*, *55*(1), 109–119.

Gregorio, D. S., Andrea, Z., Lara, M., Ivana, A., Chiara, C., Donatella, U., & Gilberto, A. (2018). Radiocarbon dating reveals the timing of formation and development of pedogenic calcium carbonate concretions in Central Sudan during the Holocene. *Geochimica et Cosmochimica Acta*, *238*, 16–35.

Gregory, R. T., Douthitt, C. B., Duddy, I. R., Rich, P. V., & Rich, T. H. (1989). Oxygen isotopic composition of carbonate concretions from the lower Cretaceous of Victoria, Australia: Implications for the evolution of meteoric waters on the Australian continent in a paleopolar environment. *Earth and Planetary Science Letters*, *92*(1), 27–42. https://doi.org/10.1016/0012-821x(89)90018-6

Han, W., Fang, X., Ye, C., Teng, X., & Zhang, T. (2014). Tibet forcing Quaternary stepwise enhancement of westerly jet and central Asian aridification: Carbonate isotope records from deep drilling in the Qaidam salt playa, NE Tibet. *Global and Planetary Change*, *116*(3), 68–75. https://doi.org/10.1016/j.gloplacha.2014.02.006

Hardie, L. A. (2003). Secular variations in Precambrian seawater chemistry and the timing of Precambrian aragonite seas and calcite seas. *Geology*, *31*(9), 785–788. https://doi.org/10.1130/g19657.1

Kakiuchi, M. and Matsuo, S. (1979). Direct measurements of D/H and 18O/16O fractionation factors between vapor and liquid water in the temperature range from 10 to 40.DEG.C. *Geochemical Journal*, *13*, 307–311. https://doi.org/10.2343/geochemj.13.307

Kim, S.-T. and O'Neil, J. R. (1997). Equilibrium and nonequilibrium oxygen isotope effects in synthetic carbonates. *Geochimica et Cosmochimica Acta*, *61*, 3461–3475. https://doi.org/10.1016/s0016-7037(97)00169-5

Kong, F., Zheng, M., Hu, B., Wang, A. Ma, N., & Ma, N., Sobron, P. 2018). Dalangtan Saline Playa in a hyperarid region on Tibet Plateau: I. evolution and environments. *Astrobiology*. *18*(10), 1243–1253. https://doi.org/10.1089/ast.2018.1830

Miller, D. L., Mora, C. I., & Driese, S. G. (2007). Isotopic variability in large carbonate nodules in Vertisols: Implications for climate and ecosystem assessments. *Geoderma*, *142*(1), 104–111. https://doi.org/10.1016/j.geoderma.2007.08.007

Mook, W. G., Bommerson, J. C. and Staverman, W. H. (1974) Carbon isotope fractionation between dissolved bicarbonate and gaseous carbon dioxide. *Earth and Planetary Science Letters*, *22*, 169–176. https://doi.org/10.1016/0012-821x(74)90078-8

Morse, J. W., Arvidson, R. S., & Lüttge, A. (2007). Calcium carbonate formation and dissolution. *Chemical Reviews*, *107*(2), 342–381. https://doi.org/10.1021/cr050358j

Mozley, P. S., and J. M. Davis, (2005). Internal structure and mode of growth of elongate calcite concretions: Evidence for small-scale, microbially induced, chemical heterogeneity in groundwater. *Geological Society of America Bulletin*, *117*(11), 1400. https://doi.org/10.1130/b25618.1

Németh, P., Mugnaioli, E., Gemmi, M., Czuppon, G., Demény, A., & Spötl, C. (2018). A nanocrystalline monoclinic $CaCO_3$ precursor of metastable aragonite. *Science Advances*, *4*(12), eaau6178. https://doi.org/10.1126/sciadv.aau6178

Prager, E. J., & Ginsburg, R. N. (1989). Carbonate nodule growth on Florida's outer shelf and its implications for fossil interpretations. *PALAIOS*, *4*(4), 310–312. https://doi.org/10.2307/3514555

Rabenhorst, M. C., Wilding, L. P., & West, L. T. (1984). Identification of pedogenic carbonates using stable carbon isotope and microfabric analyses. *Soil Science Society of America Journal*, *48*, 125–132. https://doi.org/10.2136/sssaj1984.03615995004800010023x

Rieser, A. B., Neubauer, F., Liu, Y., & Ge, X. (2005). Sandstone provenance of north-western sectors of the intracontinental Cenozoic Qaidam basin, western China: Tectonic vs. climatic control. *Sedimentary Geology*, *177*(1), 1–18. https://doi.org/10.1016/j.sedgeo.2005.01.012

Ries, J. B. (2004). Effect of ambient Mg/Ca ratio on Mg fractionation in calcareous marine invertebrates: A record of the oceanic Mg/Ca ratio over the Phanerozoic. *Geology*, *32*(11), 981–984. https://doi.org/10.1130/g20851.1

Ries, J. B. (2011). Skeletal mineralogy in a high-CO_2 world. *Journal of Experimental Marine Biology and Ecology*, *403*(1–2), 54–64. https://doi.org/10.1016/j.jembe.2011.04.006

Sancheznavas, A., Martinalgarra, A., Rivadeneyra, M. A., Melchor, S., & Martinramos, J. D. (2009). Crystal-growth behavior in Ca-Mg carbonate bacterial spherulites. *Crystal Growth & Design*, *9*(6), 2690–2699.

Stack, K. M., Grotzinger, J. P., Kah, L. C., Schmidt, M. E., Mangold, N., Edgett, K. S., et al. (2014). Diagenetic origin of nodules in the Sheepbed member, Yellowknife Bay formation, Gale crater, Mars. *Journal of Geophysical Reserach Planets*, *119*(7), 1637–1664. https://doi.org/10.1002/2014je004617

Sun, Y., Li, Y., Li, L., & He, H. (2019). Preservation of cyanobacterial UVR-shielding pigment scytonemin in carbonate ooids formed in Pleistocene salt lakes in the Qaidam Basin, Tibetan Plateau. *Geophysical Research Letters*, *46*(17–18), 10375–10383. https://doi.org/10.1029/2019gl083321

Tabor, N. J., Montañez, I. P., Steiner, M. B., & Schwindt, D. (2007). $\delta^{13}C$ values of carbonate nodules across the Permian–Triassic boundary in the Karoo Supergroup (South Africa) reflect a stinking sulfurous swamp, not atmospheric CO_2. *Palaeogeography, Palaeoclimatology, Palaeoecology*, *252*(1–2), 370–381. https://doi.org/10.1016/j.palaeo.2006.11.047

Talbot, M. R. (1990). A review of the palaeohydrological interpretation of carbon and oxygen isotopic ratios in primary lacustrine carbonates. *Chemical Geology: Isotope Geoscience Section*, *80*(4), 261–279. https://doi.org/10.1016/0168-9622(90)90009-2

Warren, J. K. (2006). *Evaporites: Sediments, Resources and Hydrocarbons*, Berlin, Heidelberg: Springer.

Wieder, M., & Yaalon, D. (1982). Micromorphological fabrics and developmental stages of carbonate nodular forms related to soil characteristics. *Geoderma*, *28*(3–4), 203–220. https://doi.org/10.1016/0016-7061(82)90003-9

Wiens, R. C., Rubin, D. M., Goetz, W., Fairén, A. G., Schwenzer, S. P., Johnson, J. R., et al. 2017). Centimeter to decimeter hollow concretions and voids in Gale Crater sediments, Mars. *Icarus*, *289*, 144–156. https://doi.org/10.1016/j.icarus.2017.02.003

Xiao, L., Wang, J., Dang, Y., Cheng, Z., Huang, T., Zhao, J., et al. (2016). A new terrestrial analogue site for Mars research: The Qaidam Basin, Tibetan Plateau (NW China). *Earth-Science Reviews*, *164*, 84–101.

Yang, Y., Fang, X., Koutsodendris, A., Ye, C., Yang, R., Zhang, W., et al. (2016). Exploring Quaternary paleolake evolution and climate change in the western Qaidam Basin based on the bulk carbonate geochemistry of lake sediments. *Palaeogeography, Palaeoclimatology, Palaeoecology*, *446*, 152–161. https://doi.org/10.1016/j.palaeo.2016.01.021

Yoshida, H., Hasegawa, H., Katsuta, N., Maruyama, I., Sirono, S., Minami, M., et al. (2018). Fe-oxide concretions formed by interacting carbonate and acidic waters on Earth and Mars. *Science Advances*, *4*(12), eaau0872. https://doi.org/10.1126/sciadv.aau0872